Electrochimica Acta 157 (2015) 41–45 http://dx.doi.org/10.1016/j.electacta.2015.01.088

High rate capability of SiOC Ceramic Aerogels with Tailored Porosity as Anode Materials for Li-ion batteries

V.S. Pradeep [a], *D. G. Ayana* [b], *Magdalena Graczyk-Zajac* [a], *G.D. Soraru* [b], *R. Riedel* [a]

a) Technical University Darmstadt, Jovanka-Bontschits-Straße 2, 64287, Darmstadt Germany,

b) University of Trento, Via Sommarive 9, 38123, Trento, Italy

Abstract

Porous carbon-rich SiOC ceramic aerogels have been synthesized from a linear polysiloxane cross-linked with divinyl benzene (DVB) *via* hydrosilylation reaction in presence of a Pt catalyst and acetone as the solvent. The obtained wet gels are aged in solvent followed by drying under supercritical conditions using liquid carbon dioxide. The resulting pre-ceramic aerogels are subjected to pyrolysis at 1000 °C under controlled argon atmosphere to form the desired SiOC aerogel. The synthesized SiOC ceramics contain 43 wt% of free carbon, which is segregated within amorphous SiOC matrix. The preceramic aerogels have BET surface area up to 230 m^2g^{-1} and a SSA of 180 m^2g^{-1} is maintained even after pyrolysis at 1000 °C. The electrochemical characterization reveals a high specific capacity of more than 600 mAh g^{-1} at a charging rate of C (360 mA g^{-1}) along with a good cycling stability. At a rate of 10C (3600 mA g^{-1}) the specific capacities as high as 200 mAh g^{-1} are recovered. The excellent properties of the materials are discussed with respect to their structural features. The porous nature of the carbon rich ceramics helps to accommodate the structural changes, which in turn allow a stable performance during repeated lithiation/delithiation.

Key words: Aerogels, Anodes, Polymer Derived Ceramics, Li-ion Batteries, Supercritical, Porous Ceramics

1. Introduction

Lithium ion batteries (LiB) are considered as a promising solution for various energy storage applications owing to their compactness, light weight, high efficiency and longer life span compared to other rechargeable battery types [1]. These rechargeable battery systems are currently dominating the field of portable electronic applications but there are still many hurdles to reach the goal of high power applications such as in hybrid electrical vehicles (HEVs). Carbon based materials are one of the best host materials for reversible lithium storage. There is a good compromise between volume expansion and lithium storage leading to extended battery life. In particular graphite has been long used as an anode material due to low operating potential vs lithium and favorable cycling performance. However, graphite is facing its limitation in lithium storage capacity because of the formation of a well-organized stage structure LiC_6 offering a capacity of 372 mA h g^{-1} [1-5]. Another crucial problem related to graphite is their limited rate capability during lithium insertion. There is a considerable discussion related to the reasons of these limits, mostly attributing the slower lithium insertion to the slow desolvation of ion at solid electrolyte interface (SEI) surface and SEI increasing resistance.

In comparison to graphite, porous carbon compounds are known to offer higher capacities especially at higher charging / discharging currents [7-19]. In particular, mesoporous carbon compounds are reported to be an interesting anode materials for high rate applications. The important features for these materials are their controlled porous structure with better interconnectivity between the pores allowing fast ion diffusion. In order to maintain the rate capability along with longer cycling life time, the host structure should also be mechanically flexible to allow uninterrupted insertion and extraction of lithium ions during the entire charging/discharging process.

Most common methods adapted for the synthesis of porous carbon materials are by using sacrificial templates [11, 20]. Another possible way for the synthesis of porous materials is based on aerogel technique. Aerogels have got much more attention since the successful synthesis of silica aerogels by Kistler in 1931[21]. Aerogels are tailor made porous networks with high surface area and relatively low densities. These materials are well known for different potential applications such as for thermal insulation, sensors, waste management, in capacitors, catalysts etc. due to their excellent properties such as high surface area, high porosity, low bulk density and low thermal conductivity [21-24]. However, the investigation of the use of carbon aerogels towards application as anode materials in lithium ion batteries is very limited [19, 23, 25, 26].

Polymer derived ceramics (PDC's) such as SiOC, SiCN etc. have been analyzed in detail for lithium storage applications. Silicon oxycarbides are ceramic structures with silicon bonded to both oxygen and carbon simultaneously. The structure of SiOC, beside the amorphous silicon oxycarbide network -in which Si atoms share bonds with O and C atoms simultaneously- contains an interconnected disordered free carbon phase which accounts for many of their excellent mechanical and electrochemical properties [27-30].

In the present work, we focus on the electrochemical properties of carbon-rich SiOC ceramic aerogels prepared by pyrolysis of low-density preceramic aerogels, obtained cross-linking, a pre-ceramic polymer under highly diluted conditions. The cross-linking of the precursor is performed via hydrosilylation reaction, using divynil benzene as crosslinking agent. The wet aerogels are supercritically dried using CO_2 and pyrolyzed at 1000 °C to produce the studied SiOC aerogel [31, 32]. The synthesized porous SiOC ceramic is subjected to electrochemical characterizations and demonstrates promising properties in particular for high rate applications.

2. Experimental Part

2.1 Material Synthesis

Starting materials, a linear polyhydridomethyl siloxane (PHMS, MW= 1900), which contains Si-H bonds, and divinylbenzene, (DVB, technical 80%, mixed isomers) were purchased from Alfa Aesar (AlfaAesar, Ward Hill, MA, USA). Platinum divinyltetramethyldisiloxane complex, ~Pt 2% in xylene (Sigma-Aldrich, St. Louis, MO, USA) was used as catalyst for the hydrosilylation reaction between the Si-H moieties of the siloxanes and the vinyl groups of the crosslinker. In a typical preparation, PHMS is cross-linked with DVB in presence of acetone as solvent using the platinum catalyst (always 5 ppm relative to Si compound). The amount of solvent is calculated assuming the 80% of porosity of the final gel [31]. The cross linking is carried out at a temperature of 150 °C in an autoclave. The autoclave is then cooled down to room temperature and the gels are transferred to a beaker with excess acetone solvent. The obtained gels are aged for one week in acetone. At the end the gels were washed by solvent exchanged up to 3 times ~~in~~ a day ~~time~~ ~~at frequent intervals~~ to remove excess of catalysts and unreacted residues. The wet gels are dried supercritically using solvent exchange with liquid CO_2. The dried gels are then pyrolysed using an alumina tubular furnace (Lindberg/Blue) under 150 mL/min of flowing argon. The samples are heated at a rate of 5 °C /min up to 1000 °C and maintained for 1 h at the maximum temperature. Cooling down to room temperature is done by turning off the furnace power. The pyrolysed sample is then milled in an agate mortar and sieved with a 40 µm sieve.

2.2 Characterization

Elemental C and O is measured with Leco C and O analyzer. The porosity is analyzed using the N_2 adsorption technique with a Micrometrics equipment, ASAP Model 2010, Norcross, GA, USA (N_2 adsorption at 77 K). The specific surface area was determined using the BET equation [33] and the pore size distribution (PSD) was obtained from the desorption

branch of the isotherm using the Barrett– Joyner–Halenda (BJH) method[34]. Assuming that the pores are cylindrical and open at both ends, the average pore size, expressed in nanometres, of a given sample is calculated using the equation 4000 TPV/SSA. The microstructure of the samples are studied using a Supra 40 Zeiss FE-SEM (Carl Zeiss NTS GmbH, Oberkochen,Germany).

Electrochemical characterization is carried out using a Swagelok® type cell assembly with lithium metal as the counter/reference electrode(99.9% purity, 0.75 mm thick, Alfa Aesar, Germany) and 1M $LiPF_6$ in ethylene carbonate and diethyl carbonate mixture of volume ratio 1:1 (LP 30, Merck KGaA, Germany) as the electrolyte. A Whatman^{TM} quartz microfiber filter (QMA, UK) separator is used between the electrodes. The working electrode is made of 85wt% of SiOC +10wt% polyvinylidenefluoride (PVDF, SOLEF, Germany) + 5wt% Carbon Black Super P® (Timcal Ltd., Switzerland) black. The mixture is made in the form of a slurry using N-methyl pyrolidone (NMP, BASF, Germany) as solvent and the slurry is then coated on an ultrathin copper foil (10 µm, Copper SE-Cu58, Schlenk Metall-folien Gmbh & Co KG). The coating is allowed to dry at 80 °C overnight and electrodes of size 7 mm is then cut from the coating. The obtained electrodes are weighed to find out the active mass of the SiOC material and then dried under vaccum at 80 °C for 24 hrs using a Buchi oven. The electrodes are then transformed in to an argon filled glovebox (MBraun) for cell assembly.

The assembled cells are subjected to galvanostatic charging/discharging studies with in a potential window of 0.005-3V with different current densities. The current densities are increased step by step after specified number of cycles and from a faster charging rate of C-rate to 10C rate. The GCPL cycling rates used are C*50 + 2C*50 +5C*50 + 10C*50 + C*20 + 2C*20. Each discharging is performed using the corresponding charging rate (C=D=360 mA g^{-1}).

3. Results and Discussion

The elemental Si, C, and O composition of the studied sample is represented in **Table 1**. Silicon content is calculated as difference to 100 wt% from both C and O wt% assuming hydrogen is present only in negligible amount. From the measured chemical composition the amount of silicon oxycarbide glass ($SiC_xO_{2(1-x)}$) and free carbon can be evaluated following a well established procedure [35]

C (wt. %)	O (wt. %)	Si (wt. %)	Si C_x O $_{2(1-x)}$ (wt. %)	Free Carbon (wt. %)
43.04	27.08	29.88	60	40

Table 1. Elemental composition of Si, C and O in final SiOC ceramics

The elemental analysis shows an increased oxygen content and relatively more wt% of mixed SiOC units for the studied aerogel sample compared to the previously studied dense samples of similar origin [36] suggesting that the processing route have an impact on the composition of final ceramics: the aerogel approach is somehow increasing the O/Si ratio of final ceramics. The free carbon content of the pyrolysed SiOC ceramics is around 40 wt%. The composition of dense samples of similar origin prepared in the conventional way amounts 49 wt.% of free carbon and 51 wt.% of amorphous SiOC mixed phase[36].

The N_2 adsorption analysis gives information on the surface area, pore size and pore volume. **Fig. 1** represents the adsorption-desorption isotherms and pore size distribution curves (inset) of the samples before and after pyrolysis at 1000 °C. The isotherm falls in class IV according to the IUPAC nomenclature representing mesoporous nature of this material. At lower pressures (P/Po\0.04)?? you mean P/P0≤0.04? the isotherms are not linear which signifies the presence of micropores in the material.[37]. The isotherms do not show a well-defined saturation plateau, indicating the presence of a considerable fraction of macropores.

Accordingly, the microstructure of the SiOC aerogels consists of hierarchical porosity, which spans from the micro to meso to macropores. The details are reported in **Table 2.** The dried gels have a surface area of 227 $m^2 g^{-1}$ with average pore size of 52 nm and the samples retains a surface area of around 180 $m^2 g^{-1}$ after pyrolysis at 1000 °C with average pore size of 24 nm.

FE-SEM micrographs are presented in **Fig. 2**. These pictures confirm the porous structure of the aerogel samples before and after pyrolysis. The homogeneous pores distribution through entire matrix is seen. The SEM image of the 1000 °C pyrolysed samples reveals that a part of porosity still remains in the final SiOC ceramics.

Temperature	**Surface area ($m^2 g^{-1}$)**	**Pore volume (cc g^{-1})**	**Pore size (nm)**
Pre-ceramic Aerogel (RT)	227	1.37	52
SiOC aerogel (1000 °C)	180	1.09	24

Table 2. BET surface area, pore volume and average pore size of studied samples

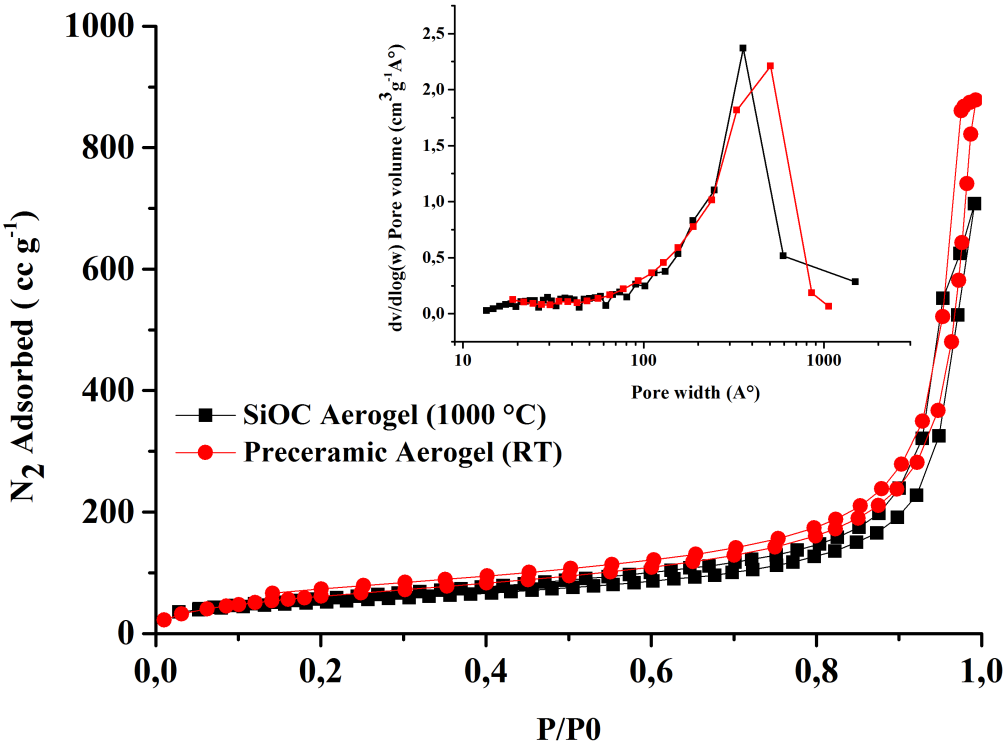

~~For the PSD curves you should use a log scale such as in this fig. Everything else in your figure is fine, do not change anything else.~~

Figure 1. Adsorption/desorption isotherm of samples before and after pyrolysis. Inset shows the pore size distribution, the data for plotting is taken from the desorption branch of isotherm.

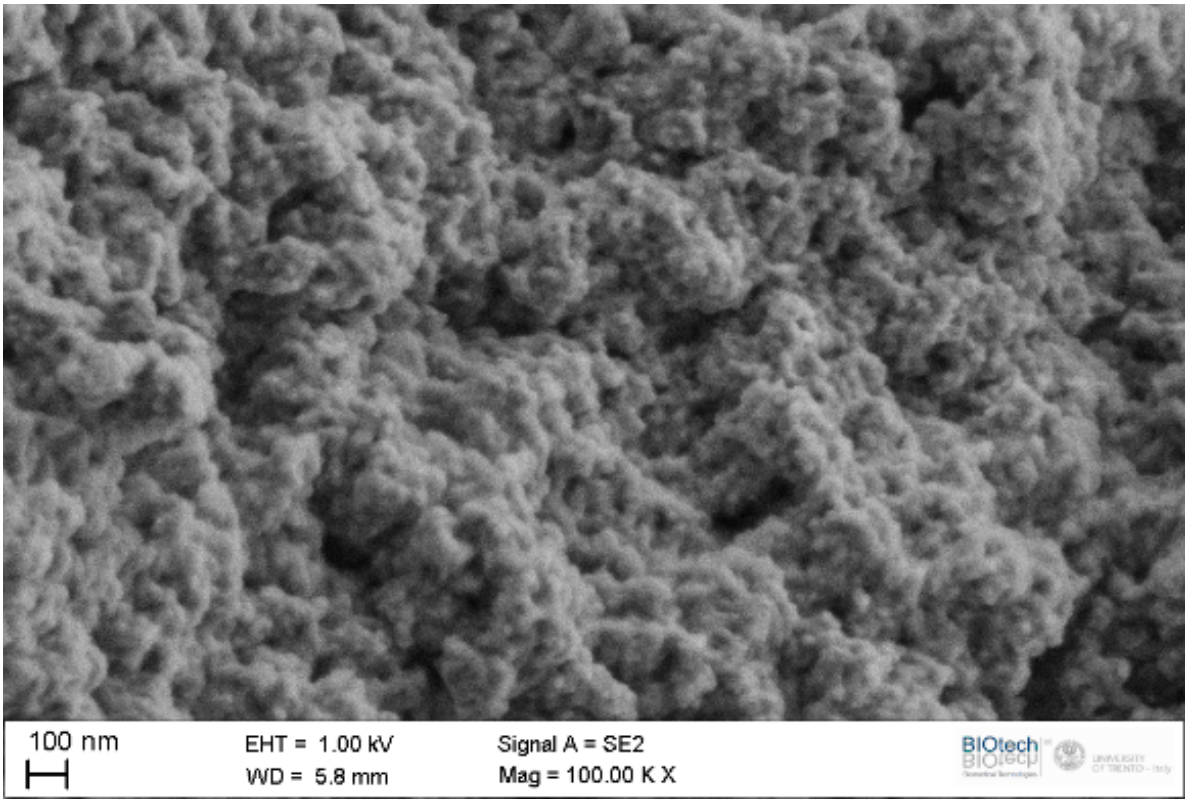

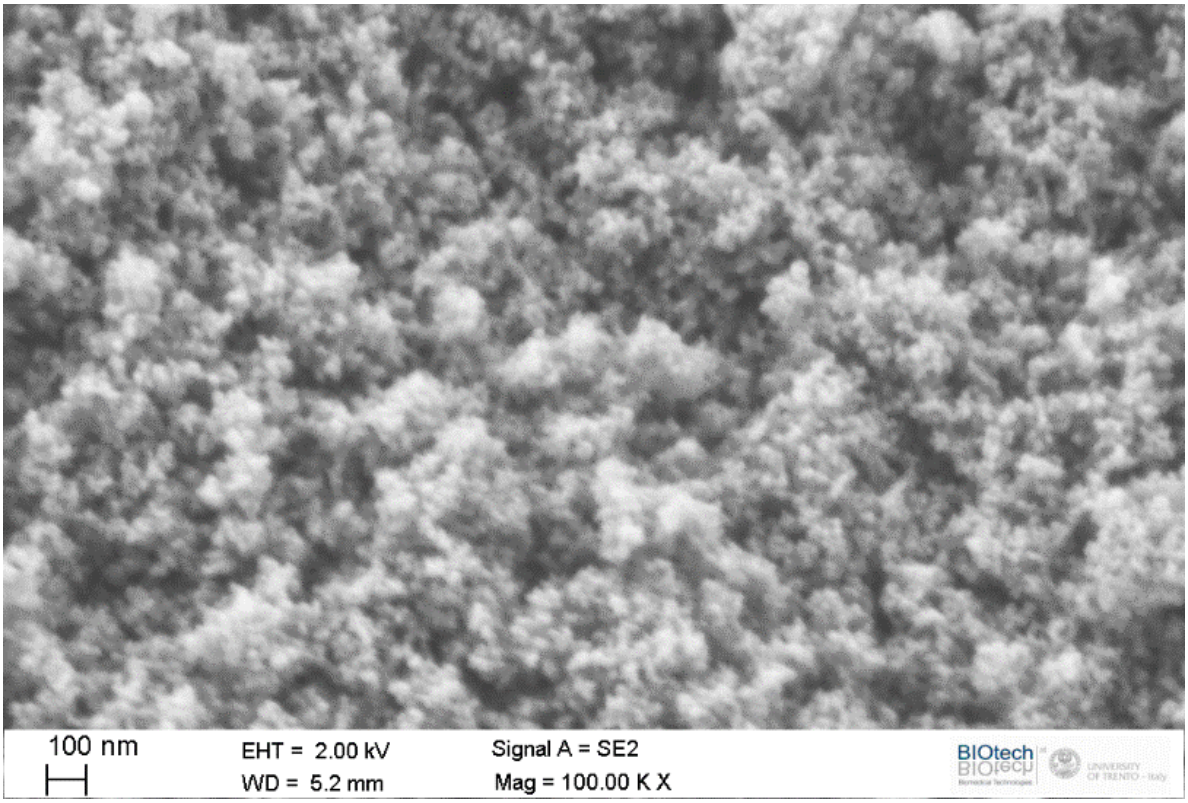

Figure 2. SEM images of studied SiOC aerogel sample a) samples before pyrolysis and b) sample pyrolysed at 1000 °C.

NMR and Raman spectra of analogous dense compounds derived from same precursors have already been reported in our previous work showing existence of different mixed SiOC units and disordered free carbon network [36]. It is expected to have only some minor changes in the Si NMR related to the increased oxygen content in the sample compared to the dense analogues.

3.1. Electrochemical Characterization

Figure 3 represents the galvanostatic charging/discharging profile for different cycles. The data include insertion/extraction curves from cycle 1, cycle 25, cycle 50 and cycle 100. The main difference between these plots are the initial large irreversible capacity during first cycle which is common in case of this class of materials, which is most probably related to the electrolyte decomposition during SEI formation between 1.5 and 0.5 V. Moreover, at lower potential lithium can be irreversibly trapped in the vicinity of oxygen or bonded by different defects/dangling bonds, etc.

The drawback of the material in a view of its possible application in Li-ion batteries is still a huge hysteresis, i.e. the charge is recovered at potential much higher than lithium is inserted. Moreover, in the case of these porous materials the delithiation curve is almost straight, with recovered capacity increasing over whole potential range, from 0.005 till 3 V.

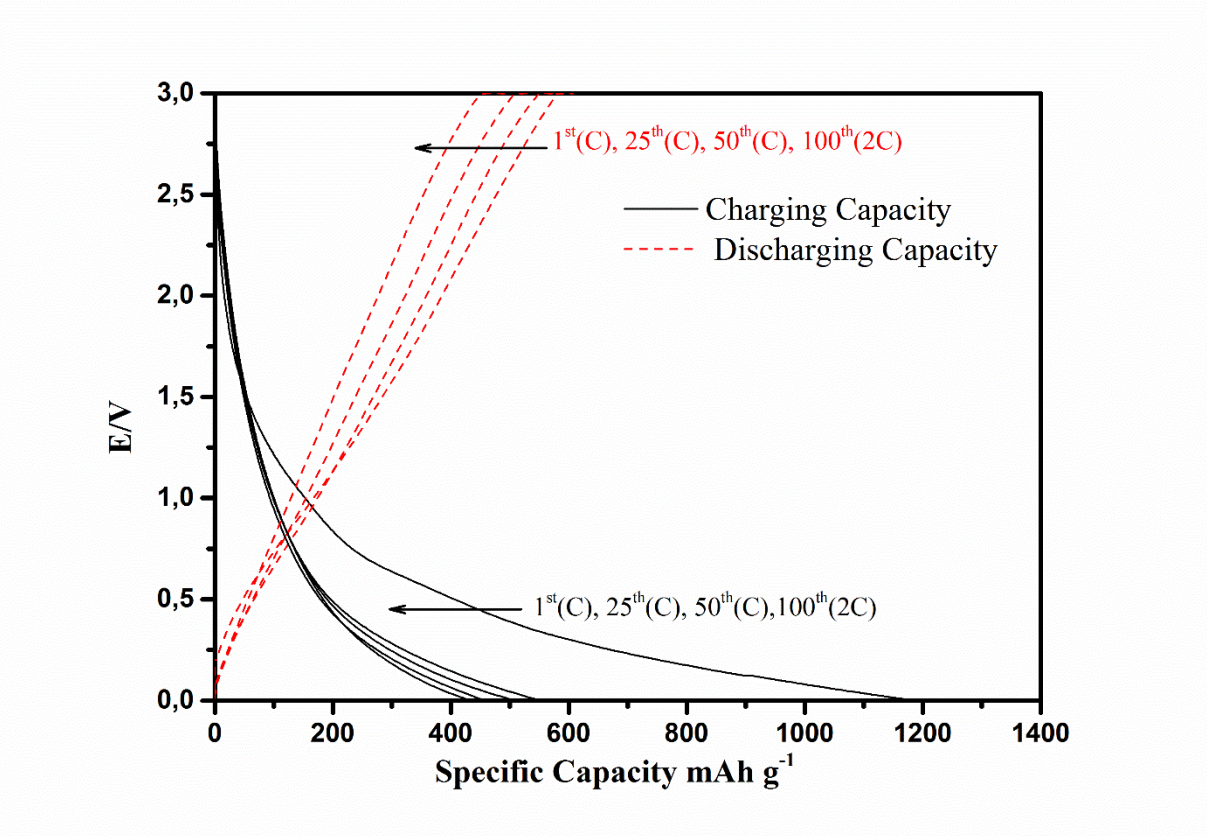

Figure 3. Charge/discharge curves of samples for 1st, 25th, 50th and 100th cycles. Charging and discharging of a specific cycle are performed always at same current rates.

Charging rate	Q Insertion (mAh g^{-1})	Q Extraction (mAh g^{-1})	Q Irreversible. (mAh g^{-1})	Efficiency (%)
C (360 mA g^{-1})	1280	600	680	49
C_{100}^{th} (2C, 720 mA g^{-1})	500	490	10	98
10C (3600 mA g^{-1})	233	232	1	99

Table 3. Specific capacities and efficiency of samples at different current rates.

Electrochemical characterization of porous SiOC anodes reveals a reversible capacity of 650 mAh g^{-1} at a charging rate of C (360 mA g^{-1}) which is almost a double of the theoretical capacity of conventional graphite anodes. The cells are also experiencing a large first cycle irreversibility similar to other disordered carbon anodes. The first cycle charge/discharge

efficiency of the sample is 50% and it increases to more than 95% in the following cycles. [36], one finds that porous SiOC deliver the capacity almost twice as high as the dense ones.

The excellent capacities at such higher rates should be interpreted in relation with the porous nature of these ceramics. Generally porous anode materials are reported to be working better at high rate regimes due to multiple reasons such as 1) the porous nature allows penetration of the electrolyte in to the deep pores and this decrease the diffusion distance of the Li ions during charging /discharging process facilitating fast Li ion storage, 2) the porous space can accommodate extra volume expansion during large amount of Li intake and 3) the high carbon content of the studied SiOC, allows the repeated lithiation/delithiation of the electrodes during multiple electrochemical cycles.

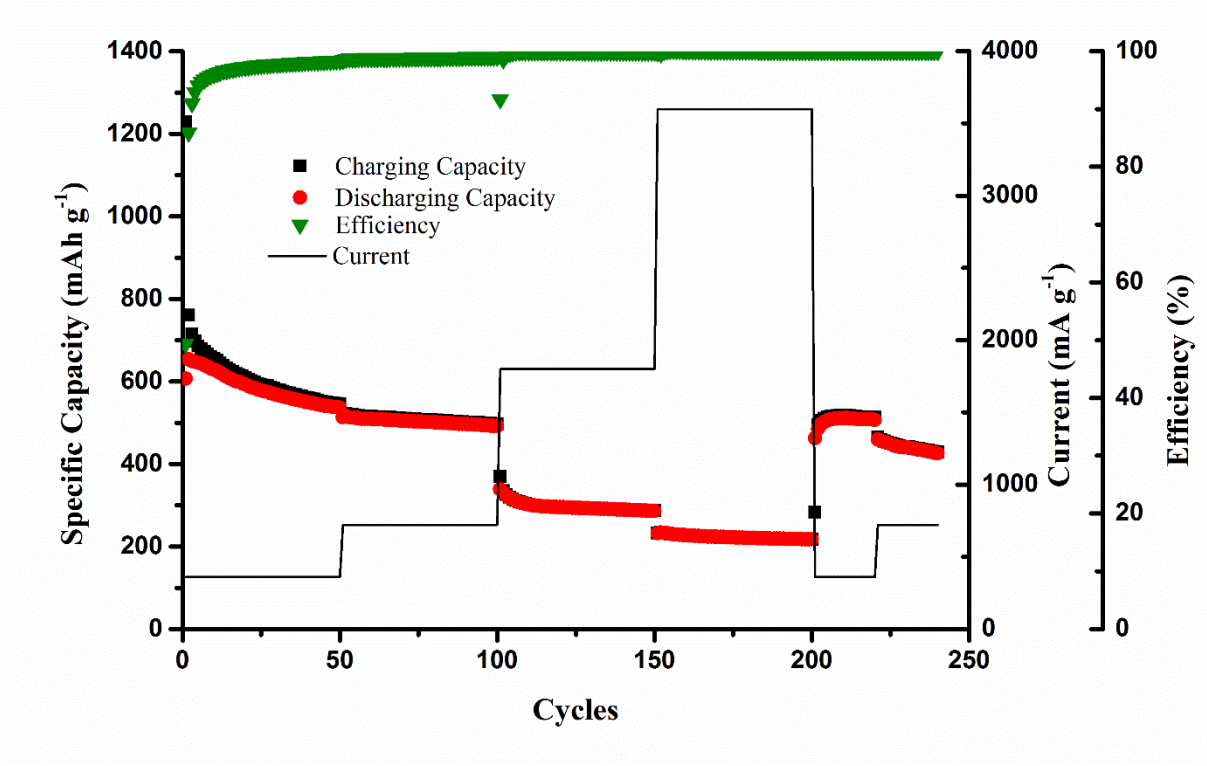

Figure 4. Cycling profile of SiOC electrode with increasing current rates plotted along with respective current densities in mA g^{-1} and % efficiency of each cycles.

The extended cycling performance is represented in Figure.4. The capacity slightly decreases during initial 20-25 cycles before gaining stability. After the initial fading the

capacity looks pretty much stable with increasing current densities. A capacity of 200 mAh g^{-1} is recovered at a rate of 10C, i.e. the cell delivers such a high capacity when charged/discharged in 6 minutes. Moreover, when switched back to slower rates of C, the initial capacity is recovered.

It is hardly possible to explain the lithium intake within the material, within both amorphous SiOC phase and free carbon phase using simple intercalation mechanism. The Li storage properties of SiOC ceramics are generally related to: (1) mixed amorphous SiOC composition (2) amount and nature of free carbon ~~content~~ (3) thermodynamic stability of the SiOC structure [36, 38-42]. The excellent rate capability of porous SiOC aerogels must be related the porous nature of the materials having an important role towards enhanced lithium diffusion. Due to the hierarchical nature of the porosity in these studied SiOC aerogels the electrolyte is able to well penetrate within the porous electrode structure, the diffusion distances which lithium ions need to cover are short and in consequence the ionic transport is fast. The porous nature of the reported SiOC aerogel sample allows for buffering the volume changes during repeated lithium insertion/deinsertion resulting in extended cycling stability especially at higher rate of charging/discharging. On the other side, the pores may also partially lead to irreversible capacity loss in terms of increased SEI losses due to large surface area and trapping of lithium ion inside the pores. There is an initial tendency of slight capacity decrease and the capacities become stable after 50 cycles. After extended cycling with gradually increasing current rates, the cells are left for charging/discharging at the initial current rate of C and the capacity is observed to be still as high as 600 mAh g^{-1} indicating the stability of the electrodes towards multiple electrochemical cycling.

4. Conclusions

Porous SiOC ceramic aerogels are synthesized in the present work from cross linked polysiloxane networks using a supercritical drying approach followed by pyrolysis at 1000 °C.

The preceramic gels have BET specific surface area up to 223 $m^2 g^{-1}$ and a surface area of 180 $m^2 g^{-1}$ is observed after pyrolysis at a higher temperature of 1000 °C. The SiOC aerogels display hierarchical porosity with the simultaneous presence of micro-meso-macropores. The galvanostatic cycling studies of SiOC electrodes reveals their excellent response toward repeated lithium storage at high charging/discharging rates. Reversible lithium storage capacity as high as 650 mAh g^{-1} is recovered at a faster rate of C (360 mA g^{-1}). The excellent cycling performance at higher rates confirms that these materials could be considered as a potential candidate towards applications requiring faster charging/discharging. Specific capacity of more than 200 mAh g^{-1} is registered at a rate of 10C (3600 mA g^{-1}), where most of the conventional electrodes fails to give any capacities. The initial capacity is recovered after series of electrochemical charging/discharging cycles with increased current densities. In order to have a complete understanding of different electrochemically active sites post lithiation studies of the electrodes samples are in progress.

References

[1] M.A. J.-M. Tarascon, Nature, 414 (2001) 359-367.
[2] P.G. Bruce, B. Scrosati, J.M. Tarascon, Angewandte Chemie, 47 (2008) 2930-2946.
[3] F. Cheng, J. Liang, Z. Tao, J. Chen, Advanced Materials, 23 (2011) 1695-1715.
[4] M. Winter, J.O. Besenhard, M.E. Spahr, P. Novak, Advanced Materials, 10 (1998) 725-763.
[5] J.R. Dahn, T. Zheng, Y.H. Liu, J.S. Xue, Science, 270 (1995) 590-593.
[6] S.R. Sivakkumar, J.Y. Nerkar, A.G. Pandolfo, Electrochimica Acta, 55 (2010) 3330-3335.
[7] K.T. Lee, J.C. Lytle, N.S. Ergang, S.M. Oh, A. Stein, Advanced Functional Materials, 15 (2005) 547-556.
[8] A.R.A. Y. Ren, F. Jiao, P.G. Bruce, Journal of Americal Chemical Society, 132 (2010) 996-1004.
[9] H.S. Zhou, S.M. Zhu, M. Hibino, I. Honma, M. Ichihara, Advanced Materials, 15 (2003) 2107-+.
[10] Z.L. Wang, D. Xu, H.G. Wang, Z. Wu, X.B. Zhang, Acs Nano, 7 (2013) 2422-2430.
[11] S.H.J. R. Ryoo, M. Kruk, M. Jaroniec, Advanced Materials, 13 (2001) 677-681.
[12] L. Chen, Z. Wang, C. He, N. Zhao, C. Shi, E. Liu, J. Li, ACS applied materials & interfaces, 5 (2013) 9537-9545.
[13] S. Chen, J. Duan, M. Jaroniec, S.Z. Qiao, Journal of Materials Chemistry A, 1 (2013) 9409.
[14] Y.S. Hu, P. Adelhelm, B.M. Smarsly, J. Maier, ChemSusChem, 3 (2010) 231-235.
[15] M.S. Kim, D. Bhattacharjya, B. Fang, D.S. Yang, T.S. Bae, J.S. Yu, Langmuir : the ACS journal of surfaces and colloids, 29 (2013) 6754-6761.
[16] Y. Li, Z.Y. Fu, B.L. Su, Advanced Functional Materials, 22 (2012) 4634-4667.
[17] Y. Xing, Y. Wang, C. Zhou, S. Zhang, B. Fang, ACS applied materials & interfaces, 6 (2014) 2561-2567.
[18] J. Yang, X.-y. Zhou, Y.-l. Zou, J.-j. Tang, Electrochimica Acta, 56 (2011) 8576-8581.
[19] J. Biener, M. Stadermann, M. Suss, M.A. Worsley, M.M. Biener, K.A. Rose, T.F. Baumann, Energy & Environmental Science, 4 (2011) 656.
[20] A. Walcarius, Chemical Society reviews, 42 (2013) 4098-4140.
[21] S.S. Kistler, Nature, 127 (1931) 741.
[22] F.S. M. Schmidt, Journal of Non-Crystalline Solids, 225 (1998) 364-368.
[23] J.C.F. R.W. Pekala, C.T. Alviso, T.D. Tran, S.T. Mayer, J.M. Miller, B. Dunn, Journal of Non-Crystalline Solids, 225 (1998) 74–80.
[24] J.L. Gurav, I.-K. Jung, H.-H. Park, E.S. Kang, D.Y. Nadargi, Journal of Nanomaterials, 2010 (2010) 1-11.
[25] G. Dayong, S. Jun, L. Nianping, W. Guangming, Z. Bin, Z. Zhihua, N. Xingyuan, Journal of Reinforced Plastics and Composites, 30 (2011) 827-832.
[26] F. Hao, Z. Zhang, L. Yin, ACS applied materials & interfaces, 5 (2013) 8337-8344.
[27] P. Colombo, G. Mera, R. Riedel, G.D. Sorarù, Journal of the American Ceramic Society, (2010) no-no.
[28] G.D. Soraru, L. Pederiva, M. Latournerie, R. Raj, Journal of the American Ceramic Society, 85 (2002) 2181-2187.
[29] P. Dibandjo, S. Diré, F. Babonneau, G.D. Soraru, Journal of Non-Crystalline Solids, 356 (2010) 132-140.
[30] Y.D. Blum, D.B. MacQueen, H.-J. Kleebe, Journal of the European Ceramic Society, 25 (2005) 143-149.
[31] G.D. Sorarù, F. Dalcanale, R. Campostrini, A. Gaston, Y. Blum, S. Carturan, P.R. Aravind, Journal of Materials Chemistry, 22 (2012) 7676.
[32] Y. Blum, G.D. Sorarù, A.P. Ramaswamy, D. Hui, S.M. Carturan, R. Riedel, Journal of the American Ceramic Society, 96 (2013) 2785-2792.
[33] H.E. S. Brunauer, E. Teller, J. Am. Chem. Soc., 60 (1938) 309-319.
[34] L.G.J. E.P. BARRETT, P.P. HALEN, J. Am. Chem. Soc.,, 73 (1951) 373-380.
[35] G.D.A. G.D. Sorau, R. Campostrini, F. Babonneau, G. Mariotto, J. Am. Ceram. Soc., 78 (1995) 379-387.
[36] V.S. Pradeep, M. Graczyk-Zajac, R. Riedel, G.D. Soraru, Electrochimica Acta, 119 (2014) 78-85.
[37] P.R. Aravind, G.D. Soraru, Microporous and Mesoporous Materials, 142 (2011) 511-517.

[38] H. Fukui, H. Ohsuka, T. Hino, K. Kanamura, ACS applied materials & interfaces, 2 (2010) 998-1008.
[39] X. Liu, M.-C. Zheng, K. Xie, Journal of Power Sources, 196 (2011) 10667-10672.
[40] V.S. Pradeep, M. Graczyk-Zajac, M. Wilamowska, R. Riedel, G.D. Soraru, Solid State Ionics, 262 (2014) 22-24.
[41] D. Ahn, R. Raj, Journal of Power Sources, 196 (2011) 2179-2186.
[42] D. Ahn, R. Raj, Journal of Power Sources, 195 (2010) 3900-3906.